Sampling Characteristics of an Aircraft-Borne Aerosol Inlet System

M. HERMANN, F. STRATMANN, M. WILCK, AND A. WIEDENSOHLER

Institute for Tropospheric Research, Leipzig, Germany

(Manuscript received 14 June 1999, in final form 18 February 2000)

ABSTRACT

When sampling aerosol particles from aircraft, the inlet system is the most critical item because it can strongly modify the number concentration, size distribution, and chemical composition of the particles. In this investigation, the authors describe a new aircraft-borne aerosol inlet and its sampling characteristics for submicrometer particle measurements in the upper troposphere and lower stratosphere. The new inlet is flown regularly on board a civil aircraft (Boeing 767 300ER) as part of the CARIBIC project. To investigate the sampling characteristics of the new inlet, a wind-tunnel study has been performed. Furthermore, particle transport losses in the sampling line have been calculated. Combining these results, an overall size-resolved inlet system sampling efficiency is given.

During transport of the aerosol from the ambient environment to the measurement devices inside the aircraft, the aerosol experiences a strong heating within a few tenths of a second. To estimate the effects of this heating on the size distribution of the sampled particles, model calculations have been performed assuming the sampled particles to consist of sulfuric acid and water. The results show that a significant amount of water evaporates from the sampled particles, whereas sulfuric acid evaporation is so slow that it is negligible for particles larger than 4 nm.

1. Introduction

In situ aircraft-borne aerosol measurements need an inlet system that transports the aerosol particles from the environment to the measurement devices inside the aircraft. Thereby, two major requirements should be fulfilled by the inlet system (cf. Baumgardner et al. 1991). First of all, the particle number concentration at the measurement devices should be the same as it is outside the aircraft (representative sampling). Second, no evaporation of or condensation on sampled particles should occur during the transport from outside to inside the aircraft (no particle modification). On aircraft, inlets can encounter air velocities of up to 250 m s^{-1}, which must be slowed down to a few meters per second to mount for the needs of the measurement devices. Furthermore, in the upper troposphere and lower stratosphere, the aerosol experiences heating of up to 80 K within tenths of a second during the transport into the aircraft. As it is not possible to avoid aerosol modification under these extreme conditions, it is desirable to quantify how the inlet system modifies the particle number concentration and number size distribution. However, knowledge about inlet sampling characteristics is usually limited or not available at all for inlet systems discussed in the literature.

In this paper, we present experimental and modeling results for the sampling characteristics of a new aircraft-borne aerosol inlet system. This inlet system has been flown regularly on board a civil aircraft (LTU International Airways) since 1997 in the CARIBIC project (Civil Aircraft for Remote Sensing and In-Situ-Measurements in the Troposphere and Lower Stratosphere Based on the Instrumentation Container Concept; Brenninkmeijer et al. 1999). The goal of this project is the simultaneous measurement of trace gases (e.g., CO, O_3, CH_4, CFCs, HCFCs) and aerosol particles (number concentration and chemical composition) in the upper troposphere and lower stratosphere. This atmospheric region is of special scientific interest, particularly because the stratosphere–troposphere exchange processes play an important role in atmospheric chemistry and climate change (cf. Holton et a1. 1995; Mahlman 1997). The measured data might serve as important input parameters for chemical and climate modeling, and give insight into this relatively unknown region of the atmosphere.

The CARIBIC system consists of the CARIBIC aircraft (Boeing 767 300ER, D-AMUN) a modified standard air freight container ($2.5 \times 1.8 \times 1.6$ m) containing the measurement devices, and the inlet system described here. During measurement flights, the CARIBIC container is located in the B-767's forward cargo com-

Corresponding author address: Markus Hermann, Institute for Tropospheric Research, Permoserstrasse 15, D-04318 Leipzig, Germany. E-mail: hermann@tropos.de

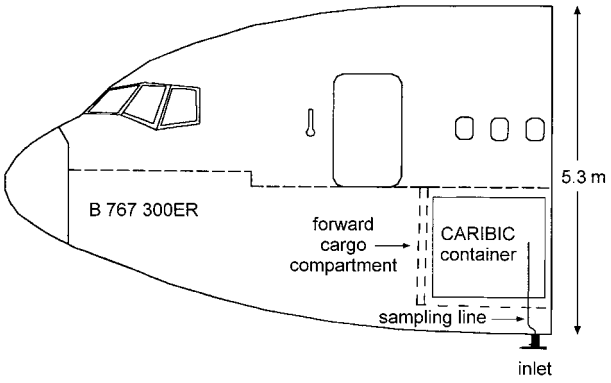

FIG. 1. CARIBIC aircraft, measurement container, and inlet system. The latter consists of the inlet, mounted at the lower B-767 fuselage directly below the container, and the sampling line, connecting the inlet with the container.

partment, directly above the inlet (cf. Fig. 1). The aerosol unit of CARIBIC consists of three modified condensation particle counters (CPCs) with lower detection limits of 4, 12, and 18 nm, respectively. To analyze the chemical composition of the particles, a particle sampler with 14 sequentially activated parallel impactors is located in the unit. It samples all particles larger than approximately 65 nm at flight level pressure.

In section 2 we discuss the major sampling problems in aircraft-borne particle measurements. The design of the CARIBIC inlet itself will be presented in the section 3. Thereafter, a wind-tunnel calibration setup will be described, which has been used to investigate the transmission efficiency of the inlet (section 4). Section 5 discusses the results obtained from these wind-tunnel studies. Furthermore, calculated transport efficiencies and the modeling results dealing with the particle modifications caused by the heating of the aerosol in the sampling line will be shown. A summary of the results is given in section 6.

2. Sampling problems

Airborne inlet systems can be subdivided into two parts: the inlet itself and the sampling line connecting the inlet to the measurement devices. In Fig. 1 the CARIBIC sampling system is shown as an example. The inlet is mounted at the lower aircraft fuselage and connected to the measurement devices by a 2-m-long stainless steel tube with 4-mm inner diameter.

Likewise, the overall sampling efficiency of an inlet system can be subdivided into the inlet efficiency and the transport efficiency of the sampling line. The inlet efficiency describes what fraction of a given particle size enters the inlet (aspiration efficiency) and how well this fraction is transmitted through the inlet (transmission efficiency). Possible particle modifications are not accounted for in these efficiencies.

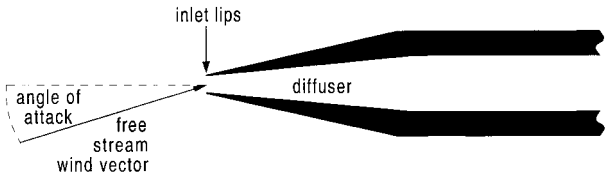

FIG. 2. Sketch of a diffuser-type inlet.

a. Aspiration efficiency

There are several aspiration effects that might lead to a decrease as well as to an enhancement of particles in the sample volume relative to the freestream particle concentration (cf. Baumgardner et al. 1991). Airborne aerosol inlets must be mounted at aircraft fuselage points, where the influence of the aircraft on the sample aerosol is minimal. As it is desirable to sample the aerosol from the undisturbed freestream, the inlet should be mounted well outside the aircraft boundary layer. Furthermore, at regions of strong curvature (e.g., the aircraft nose) trajectories of large particles might not follow the streamlines anymore, which leads to shadow or enhancement zones around the aircraft (King et al. 1984; King 1984, 1985, 1986; Geller et al. 1993; Towhy and Rogers 1993). This effect is only important for particles or droplets larger than ca. 10 μm and can consequently be neglected for submicrometer particles (King 1984; Twohy and Rogers 1993).

Anisokinetic sampling can also lead to aspiration problems. For subisokinetic (freestream velocity $>$ sampling velocity in the inlet) as well as for superisokinetic (freestream velocity $<$ sampling velocity) conditions particle depletion and enhancement can occur (Willeke and Baron 1993). In this context, it is important to note that air velocities in the vicinity of the aircraft fuselage may be different from freestream values. Further aspiration problems arise due to anisoaxial sampling, where a nonzero angle between the inlet and the freestream streamlines exists. Anisoaxial sampling can occur due to the influence of the aircraft on the streamlines, but also due to the fact that the aircraft ''rides'' on the air and therefore always a certain angle between the aircraft centerline and the freestream streamlines exists (cf. Fig. 2). This so-called angle of attack (in the figure exaggerated to show the effect) depends on flight conditions and is not constant. Since sampling errors due to anisokinetic and anisoaxial sampling are based on particle inertia, they are only important for droplets or larger particles.

b. Transmission efficiency

In connection with the angle of attack, the design of the inlet lips (the edge of the inlet tip, cf. Fig. 2) can lead to particle losses or gains in the inlet. In general, there are two possibilities of designing inlet lips: blunt, round ones, or sharp ones. The advantage of the blunt inlet lips is that they bend the streamlines at the entrance

of the inlet so that they become parallel to the inlet. One of their disadvantages is, however, that high Mach numbers may occur near the curved surface, which generate shock waves and thereby turbulence downstream (Baumgardner et al. 1991). Furthermore, because of the nonnegligible lip area, particles may impact on the lips and breakup into several smaller particles (Baumgardner et al. 1991; Hudson and Frisbie 1991; Weber et al. 1998). Sharp inlet lips, on the other hand, do not cause this particle breakup. However, as the streamlines are not bent by this type of lips, sharp lips together with a nonnegligible angle of attack may cause flow separation and turbulence inside the inlet which is associated with particle losses (Baumgardner et al. 1991).

Sharp lips also make the inlet more sensitive to electrostatic effects. From aeronautical engineering it is well known that charges may be accumulated on the aircraft fuselage, especially when flying through clouds. Because of the relatively small size of the inlet tip, this can lead to very strong and nonuniform electrical fields. It is well known that these electrical fields influence particle sampling (Willeke and Baron 1993). Because of the complexity of this topic, the magnitude of the influence has not been studied in detail and investigations have just started (Radke and Dye 1991; Romay et al. 1996). A quantification of particle losses in airborne sampling due to electrostatic effects is currently impossible. After the sampled air has entered the inlet, it has to be slowed down from up to 250 m s^{-1} to a few meters per second. This is usually achieved by means of a diffuser, that is, a cone that reduces the air velocity by increasing the cross-sectional area (cf. Fig. 2). In designing such a diffuser, it is, on the one hand, desired to minimize its length to prevent the development of a turbulent boundary layer. On the other hand, expansion ratios larger than 5 as well as expansion angles larger than 6° may cause flow separation (Baumgardner et al. 1991; Ram et al. 1995; Cain et al. 1998), which results in increasing particle losses (Huebert et al. 1990; Ivie et al. 1990).

As the rear part of most inlets consists of a tube, also all the loss processes mentioned in the following section can influence the inlet transmission efficiency.

c. Transport efficiency

The most important transport loss processes for aerosol flows in tubes are gravitational settling, laminar or turbulent diffusion, turbulent inertial deposition, and inertial deposition in bends (cf. Willeke and Baron 1993).

Gravitational settling of particles can be an important loss process for larger particles. For CARIBIC, where only submicrometer particles are investigated and the transport time from the inlet to the particle counters is less than 0.25 s, gravitational settling can be neglected. Diffusive deposition (laminar or turbulent) is always present in tube flow systems. As the tube walls act as particle sinks, a radial concentration gradient is established inside the tube which results in a particle flux toward the walls.

In turbulent flows, larger particles can additionally be propelled toward and deposited on the tube walls by eddies. This process is called turbulent inertial deposition and is only important for supermicrometer particles in turbulent flows and therefore negligible for CARIBIC.

Another process, which is due to inertial effects, is the deposition of particles in tube bends. As the air flow in tube bends rapidly changes its direction, larger particles cannot follow the streamlines and may impact on the walls (Pui et al. 1987). All these processes have been basically studied in laboratory experiments and equations to calculate these losses are available (Willeke and Baron 1993).

3. CARIBIC inlet design

In the past, different types of aircraft-mounted inlets for submicrometer particle measurements have been used. The simplest version is a tube facing reverse to flight direction, used for instance by Schröder and Ström (1997). More frequently used are diffuser-type inlets with rather sharp (Huebert et al. 1990) or blunt inlet lips (Porter and Clarke 1992; Sheridan and Norton 1998). In 1989, McFarland et al. reintroduced an old type of aerosol inlet, a shrouded probe, and investigated its performance for air velocities, which are encountered by ground-based inlets. A shroud is a cylinder that is located in front and around a classical diffuser. The shroud aligns the streamlines along the diffuser axis and therefore minimizes sampling artifacts resulting from misalignement of the streamlines (e.g., anisoaxial sampling) in the vicinity of the inlet. Shrouds can also be used to reduce the air velocity in a similar way as diffusers. Although Torgeson and Stern (1966) used this principle for aircraft-borne measurements, this type of inlet has not been frequently used until the last few years (Baumgardner et al. 1991; Ram et al. 1995; Cain and Ram 1998; Cain et al. 1998; Murphy and Schein 1998; Twohy 1998; Weber et al. 1998). Still at the beginning of their development, shrouded probes are currently the most promising aircraft-borne aerosol inlet type.

At the beginning of CARIBIC in 1994, the understanding of shrouded probes was limited and therefore a ''semiclassical'' diffuser type geometry was chosen for the inlet. A sketch of the CARIBIC inlet is shown in Fig. 3. The diffuser tube of this inlet is mounted on a strut in 20.6-cm distance and parallel to the aircraft fuselage (cf. Fig. 1). This guarantees the sampled air to be well outside the aircraft fuselage boundary layer, which is in the order of a few centimeters (Marenco et al. 1998). The position of the inlet at the aircraft fuselage and three fuselage radii away from the aircraft nose was determined mainly by feasibility and security considerations of the aircraft manufacturer instead of model calculations (e.g., black spots on the B-767's anticol-

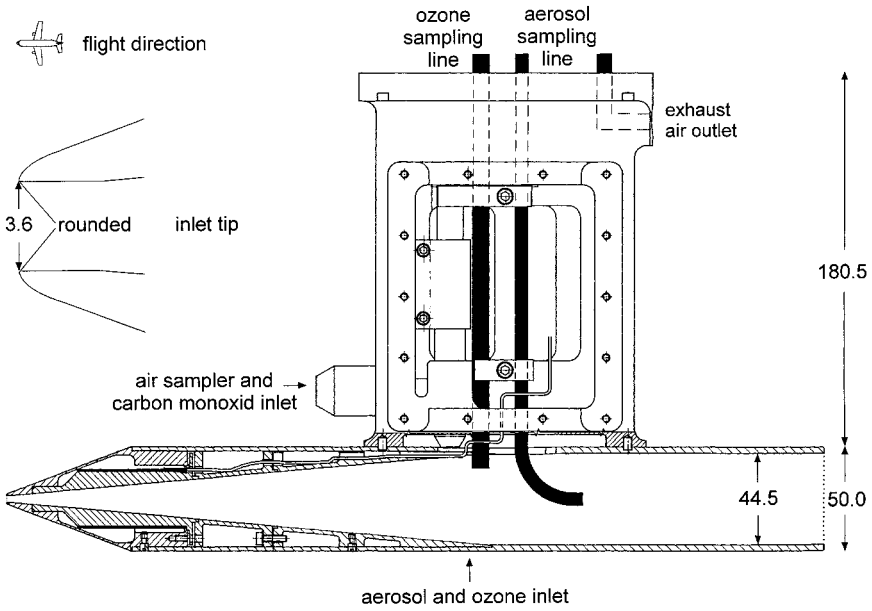

FIG. 3. Sketch of the CARIBIC inlet. Ambient, high-velocity air enters the inlet through the 3.6-mm hole at the tip and is slowed down in the diffuser. Downstream of the diffuser, a small amount of air is sucked as sampling air through a backward-facing 6-mm tube toward the measurement devices inside the aircraft. After measurement the air leaves through the exhaust air outlet. Dimensions are given in millimeters.

lision radar due to the inlet had to be prevented). In general, the mounting under the aircraft is less likely to show negative sampling effects caused by the aircraft than positions above the aircraft do, because aircraft normally fly with small positive pitch angles (cf. Geller et al. 1993). Furthermore, the positioning more than three fuselage radii downstream of the aircraft nose has the advantage that the sampling velocity is likely do be within a few percent of the freestream velocity (King 1984).

In the CARIBIC inlet system, ambient air enters the inlet through a 3.6-mm hole and flows into the diffuser. To prevent icing of this hole, the inlet tip is heated with 40-W power. The curvature of the inlet lips was chosen according to a NASA system (NACA 1-55-050, cf. Soderman et al. 1991), and represents a compromise between blunt and sharp inlet lips. These lips together with the fact that the CARIBIC B-767 normally encounters pitch angles of ca. 2° during level flight (up to 10° for research aircraft) compensate the missing shroud and keep the sampling artifacts due to misalignment minimal.

As the length of the inlet was restricted by Boeing, the diffuser's expansion angle of 10° is rather large and the expansion ratio is larger than 150. It is obvious that inside this diffuser flow separation will occur. Observations made during the inlet calibration support this assumption (cf. section 5a).

After the air velocity is slowed down to a few meters per second inside the diffuser, most of the air leaves the inlet through the rear. Only a small amount of about 10 L min^{-1} is sucked into the 4-mm (inner diameter) aerosol sampling tube, which is connected to the measurement container in the forward cargo compartment. As this tube faces backward, only small particles are sampled by the measurement system. Larger particles, droplets or ice crystals leave the inlet through the rear as they are not able to follow the 180° bend of the sample flow streamlines because of inertial effects. The backward-facing tube therefore acts as a separator. It should be noted that just in front of the aerosol sampling tube another sampling tube is located (position determined by technical requirements), which is used to extract a sample flow of 14 L min^{-1} for the ozone measurement devices of the CARIBIC container.

4. Inlet calibration

Knowledge about the upper cutoff diameter of the inlet and the particle losses inside the diffuser tube is important for properly interpreting the measurements performed using the inlet. Inlet characteristics can be determined either theoretically by means of numerical models or experimentally (in-flight comparison or wind-tunnel experiments). Until 1991 ''in no case has the internal flow of any currently-used airborne inlet been adequately modeled or measured under airborne conditions'' (Baumgardner and Huebert 1993) and this holds especially with respect to the particle losses occurring in these inlets.

Modeling of inlet sampling efficiencies is still in its early stages (Lin and Heintzenberg 1995; Ram et al.

1995; Cain and Ram 1998; Laucks and Twohy 1998; Twohy 1998) and needs experimental validation. On this account, in this study an experimental inlet characterization was chosen.

Huebert et al. (1990) performed in-flight comparisons of different diffuser-type inlets. They measured particle losses of up to 90% in aerosol mass inside the diffuser and in the connected tube bends by determining the deposited aerosol mass. Furthermore, they observed a decrease in particle transmission efficiency with increasing particle size, which is supported by the fact that deposition increases with increasing inertia. Even for the non-sea-salt sulfate, which is usually associated with submicrometer particles, they obtained transmission efficiencies not higher than 50%.

Porter et al. (1992) carried out in-flight comparisons between an optical particle counter (OPC) located downstream an inlet and a wing-mounted forward scattering spectrometer probe (FSSP), which measures the particles outside the aircraft. Furthermore, they compared their OPC data to an external filter sampler. Their data suggest that the losses for submicrometer particles are much smaller than the 50% stated by Huebert et al. (1990). Similar results were obtained by Sheridan and Norton (1998) who compared two inlets under flight conditions. They obtained transmission efficiencies of 10%–50% in aerosol mass for coarse particles and of 80%–90% for submicrometer particles. All of these studies were conducted under clear-air flying conditions.

Weber et al. (1998) did not give transmission efficiencies, but their in-flight comparison of two different inlets shows large differences in particle counts while flying in clouds. Their data suggest that the different inlet lips used for the two inlets are responsible for this discrepancy and show that further investigations on airborne aerosol inlets are necessary.

Besides in-flight comparisons of different inlets, wind-tunnel studies are the most appropriate way of investigating aircraft-borne inlets. While wind-tunnel studies in general offer the possibility of taking many measurements under controlled conditions within a short period of time, there are major problems associated with investigation of aircraft-borne inlets in wind-tunnel experiments. Specific problems are

- to find a wind-tunnel that provides 40–250 m s^{-1} wind velocity at pressures from 1000 down to 40 hPa and temperatures of $-80°$ to $+30°$C;
- to find an aerosol generation system that provides a stable aerosol, homogeneously distributed over the wind-tunnel test section under the conditions stated above; and
- to find an aerosol measurement system that has the capability to measure the aerosol under the above conditions.

These requirements cannot be met in total by currently available wind-tunnel facilities. Due to the complexity of airborne inlet wind-tunnel studies, only a few have been performed until the last years. Mainly the performance of shrouds has been investigated (Cain et al. 1998; Twohy 1998) and there are only three experiments dealing with the determination of particle transmission efficiencies. In 1990, Ivie et al. investigated supersonic particle probes for particle losses to the wall by using supermicrometer di-octylphtalate droplets. They also obtained results for subsonic diffuser sections. Sheridan and Norton (1998) used ambient aerosol to determine the transmission efficiency for coarse and fine particles. They distinguished these two size ranges by the chemical species normally associated with smaller and larger particles, respectively. Murphy and Schein (1998) also used ambient aerosol, but they measured the size of coarse and accumulation mode particles by using a PMS LasAir 1001 (0.1–2.0 μm) and a Climet 208A white light counter (0.35–9.0 μm). Summarizing the existing literature, it can be stated that (according to our knowledge) for no airborne aerosol inlet size resolved sampling or transmission efficiencies have been published up to now, except for the work of Murphy and Schein (1998). For Aitken and ultrafine mode particles (particle diameter $<$80 nm), there are no data at all.

Characterization of the CARIBIC inlet means to determine the aspiration and transmission efficiencies. To obtain the aspiration efficiency, a simulation of the flow field around the CARIBIC inlet at flight conditions is necessary. However, this would require to operate a wind tunnel of several meters size and more than 10 000 L min^{-1} volume flow. As it was not possible at our institute to build up such a large wind tunnel, this approach was abandoned and only the flow inside the inlet was simulated. This reduces the wind-tunnel inner diameter to 8 cm and the volume flow to less than 100 L min^{-1}. Consequently, only information about the transmission efficiency and none about the aspiration efficiency was obtained. However, there are several reasons why the latter can be assumed to be close to 100% for the CARIBIC inlet. The inlet is mounted well outside the aircraft fuselage boundary layer, and fine particles follow the streamlines so that neither shadow and enhancement zones nor sampling errors due to slightly anisokintec or anisoaxial sampling should occur. Furthermore, the small angles of attack together with the rounded inlet lips reduce misalignement effects.

The effect of the inlet lips on the transmission efficiency could also not be studied with this setup. However, the information on the influence of the separator on the transmission efficiency (the upper cutoff of the inlet) is gained.

Even with this smaller wind tunnel, it was not possible to simulate the real flight conditions (high aircraft velocity, low pressure, and low temperature). Therefore a similarity approach was used. This approach is based on the assumption that flow and particle transport are similar if dimensionless properties such as the Reynolds number (flow field), particle Schmidt number (diffusive particle transport), and particle Stokes number (inertial

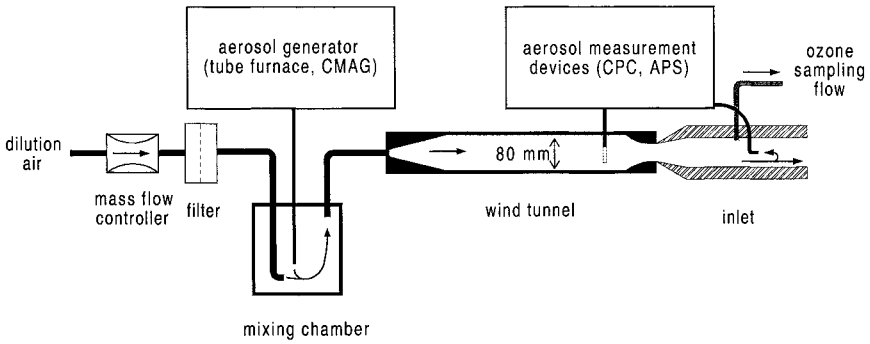

FIG. 4. Wind-tunnel calibration setup. The calibration aerosol was generated either with a tube furnace generator (Ag particles) or a condensation monodisperse aerosol generator (CMAG; Model 3475, TSI Inc., DEHS particles). In the wind tunnel and downstream the inlet, the particles were measured with a condensation particle counter (CPC; Models 3010/3025, TSI Inc.) or an aerodynamic particle sizer (APS, Model 3320, TSI Inc.). To achieve an inlet flow field as identical as possible to that under flight conditions, the flow to the ozone devices was also simulated (cf. Fig. 3).

effects) are identical in-flight and in the laboratory. The Reynolds number is given by

$$\mathrm{Re} = \frac{\upsilon d}{\nu}, \tag{1}$$

where υ the gas velocity, d the characteristic length (here the inlet tube diameter), and ν the kinematic viscosity of the gas. The Schmidt number is a measure for diffusive properties of a particle and is defined by the ratio of kinematic viscosity of the gas to the particle diffusion coefficient, D:

$$\mathrm{Sh} = \frac{\nu}{D}. \tag{2}$$

As larger particles are affected by inertial effects, the appropriated dimensionless particle property in this size range is the particle Stokes number, Stk. It is given by

$$\mathrm{Stk} = \frac{\rho_p d_p^2 \upsilon C_c}{18\eta d}, \tag{3}$$

where ρ_p and d_p are the particle density and diameter, C_c the slip correction, η the dynamic viscosity of the gas, and d the characteristic length for the given application (here, d is the diameter of the backward-facing tube).

The chosen approach holds even if the dimensional properties such as temperature, pressure, particle size, and density, etc. are different. It allows one to calibrate the inlet under conditions that can be achieved in the laboratory.

During the studies presented here, laboratory and in-flight gas Reynold number as well as particle Schmidt and Stokes numbers were set to the same values as for flight conditions. Gas Mach numbers, however, were different (0.8 in-flight, 0.3 in the laboratory). As a consequence, the dynamic heating, that is, the increase in temperature due to the deceleration of the air in the diffuser, is different for both cases (27 K in-flight, 5 K in the laboratory). The resulting difference in Re, however, is relatively small (<10%).

For the experiments, two cases were chosen that represent the two most extreme flight conditions that the inlet encounters during level flight. They are determined by the lowest and largest Reynolds number in the rear part of the inlet:

- low Re ≡ midlatitude, summer atmosphere, 39 000-ft flight altitude, 196.4-hPa pressure, 219.5-K temperature, 235 m s^{-1} true air speed, Re = 1452
- high Re ≡ midlatitude, winter atmosphere, 29 000-ft flight altitude, 318.1-hPa pressure, 228.0-K temperature, 235 m s^{-1} true air speed, Re = 2231

All data are either based on the *U.S. Standard Atmosphere* and taken from Driscoll and Vaughan (1978), or are measured data obtained from the CARIBIC B-767's aircraft communication (ARINC) system during flight.

In Fig. 4, the inlet calibration setup is shown. To cover the submicrometer and part of the supermicrometer size range, two different aerosol generators were used. Silver particles were generated in the size range from 4.5 to 50 nm using a tube furnace generator (Scheibel and Porstendörfer 1983). For the 0.5- to 6-μm diameter, DEHS particles (diethyl-hexyl-sebacate, $C_{26}H_{50}O_4$) were produced by a Condensation Monodisperse Aerosol Generator (CMAG; Model 3475, TSI Inc., St. Paul, Minnesota). To obtain a high volume flow of aerosol, the primary aerosol was diluted with particle-free air in a mixing chamber. Downstream of that chamber, the aerosol was injected into the wind tunnel. In the wind tunnel, the airflow is laminar with Reynolds numbers below 1500. At the end of the wind tunnel, the flow is accelerated to the desired air speed by a nozzle. Downstream of the wind tunnel a CARIBIC inlet mock-up was mounted, which has the same inner geometry and dimensions as the original one. Just upstream of the acceleration nozzle, a ¼-in. tube could be inserted ver-

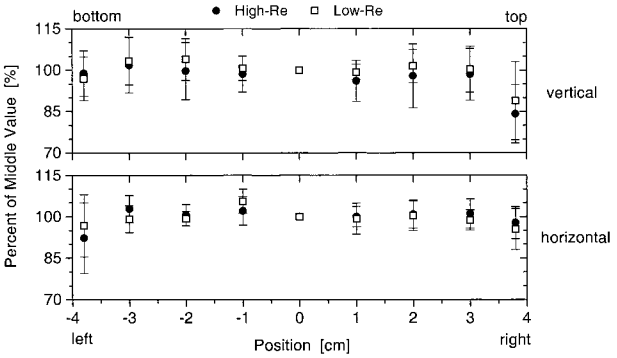

FIG. 5. Vertical and horizontal number distribution of 2-μm DEHS particles in the wind tunnel. Concentrations measured at a given position are presented as percentage of the concentration measured at the centerline of the wind tunnel. The position is given in centimeter distance relative to the centerline of the wind tunnel. Positive values represent the top or the right wall of the tunnel, respectively. Negative values correspond to the bottom or left wall.

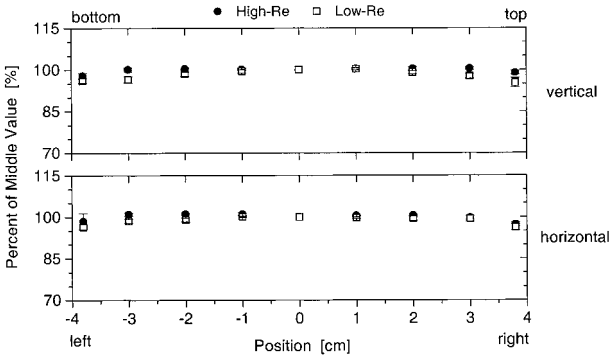

FIG. 6. Vertical and horizontal number distribution of 20-nm Ag particles in the wind tunnel. Same representation as in Fig. 5.

tically as well as horizontally as particle probe into the wind tunnel. This probe serves two purposes. First, it was used to measure the test aerosols spatial distribution over the tunnel area to guarantee a homogeneously distributed aerosol. Second, during inlet calibration, the aerosol concentration value at the centerline of the wind tunnel measured using this probe was used as reference value to which the concentration measured downstream the inlet was compared. The sampling efficiency of this reference probe was assumed to be 100%, since the wind tunnel velocity at the probe is only in the order of 20 cm s^{-1}. Consequently, the corresponding particle Stk numbers are smaller than 10^{-2} and such particles follow the streamlines of the reference sampling air. During measurements downstream the inlet the reference probe was removed to prevent turbulent particle deposition in the wind tunnel.

For the concentration measurement itself, two CPCs (Models 3010 and 3025, TSI Inc.) for small particles and an aerodynamic particle sizer (APS; Model 3320, TSI Inc.) for large particles were used.

In Fig. 5, the spatial distribution of 2-μm DEHS particles over the wind tunnel is shown for both investigated flight situations, low Re and high Re. As measure of the homogeneity, the concentration at a given position is expressed as percentage of the concentration measured at the center line of the wind tunnel. The position is measured in centimeter distance relative to the center line of the wind tunnel with an accuracy of ± 1 mm. Positive values represent the top or the right wall of the tunnel respectively, that is, the walls where the particle probe enters the wind tunnel. Negative values correspond to the bottom or left wall.

It can be seen that for both investigated flight situations the aerosol is homogeneously distributed over the wind tunnel within a few percent. The error bars represent one standard deviation. Near the walls (2 mm away) boundary layer effects can be observed. The concentration in the boundary layer, however, still exceeds 84% of the value at the center line.

Figure 6 shows the same picture for 20-nm Ag particles. The spatial distribution of the small particles is even more homogeneous, and the normalized concentrations near the wall are larger than 95%. The different standard deviations in both figures are caused by the different aerosol generation (CMAG/tube furnace) and measurement devices (APS/CPC). These results presented in Figs. 5 and 6 show that for all cases (small and large particles, low and high Re) a homogeneous distributed aerosol can be achieved in the wind tunnel by using this calibration setup.

The CARIBIC inlet transmission efficiencies were determined by the ratio of the particle concentration measured downstream of the inlet and the concentration measured inside the wind tunnel, that is, upstream of the inlet. Measurements were taken alternating several times between the wind tunnel and the inlet to account for possible concentration fluctuations of the test aerosol. The flow through the 6-mm tube in the inlet was adjusted to the same Reynolds number as under flight conditions. In the same way, the flow to the ozone devices was simulated to achieve an inlet flow field as identical as possible to that under flight conditions.

5. Results

a. Transmission efficiency

In Fig. 7, the obtained transmission efficiencies for the flight condition high Re and small particles are shown. The error bars in this and all following plots represent the experimental standard deviation. Particles which are driven to the diffuser wall hit the wall at a rather acute angle. As the Ag particles have high density, this might lead to bounce-off effects (cf., e.g., Cheng and Yeh 1979). To investigate this, in half of all experiments, the inner walls of the inlet were coated with a vacuum grease.

From Fig. 7, a decrease of the transmission efficiency for smaller particles can be seen. This behavior suggests that diffusive processes are responsible for most of the

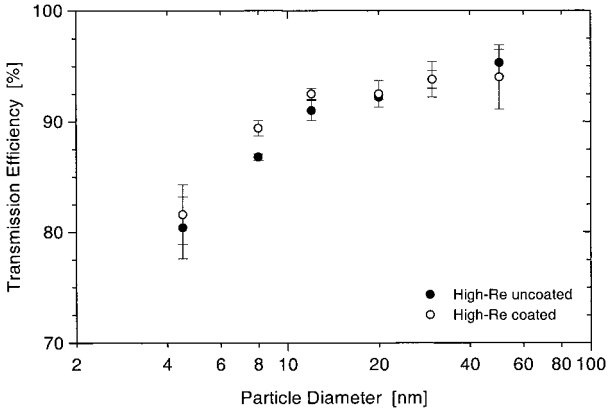

FIG. 7. Measured inlet transmission efficiencies for small particles and case high Re.

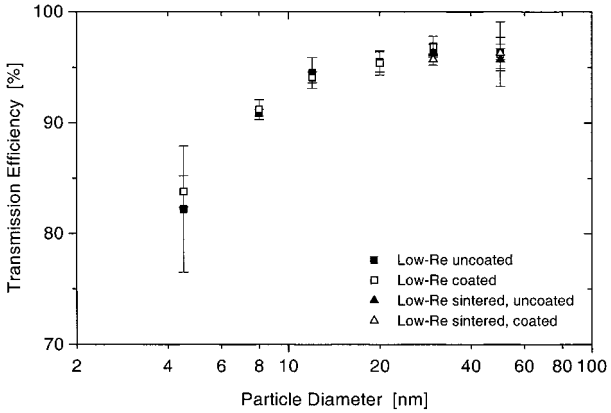

FIG. 8. Measured inlet transmission efficiencies for small particles and case low Re.

particle losses, as particle diffusion is increasing with decreasing particle size. Furthermore, from this figure it can be seen that the transmission efficiencies measured in the coated and uncoated cases agree within a few percent, that is, bounce-off effects are not relevant for the silver particles.

Figure 8 depicts results for the low Re case. Here, additional measurements have been performed with sintered 30- and 50-nm particles in order to investigate the influence of particle density on the transmission efficiency. Normally, Ag particles of that size have the shape of agglomerates and their density is much lower than the silver bulk density. However, if they are sintered in a second furnace, they shrink to nearly round, closed-packed clusters with nearly bulk density (cf., e.g., Schmidt-Ott 1988).

The results for the low-Re case again show almost no particle losses for particles larger than 30 nm, and a rapid increase of particle losses (decrease of transmission efficiency) toward smaller diameters. For 30- and 50-nm particles, the measured values agree very well for both particle densities and also the inlet coating does not influence particle transmission efficiency. This implies that the particle losses for small particles are independent of particle density and shape and depend only on particle size. Hence, as anticipated, loss processes based on particle inertia can be excluded for ultrafine and Aitken particles in our inlet.

To determine transmission efficiencies for real flight conditions, the obtained results were transformed assuming identical particle Schmidt numbers. For example, a 4.5-nm particle in the laboratory wind-tunnel experiment corresponds to a 4.7-nm particle under flight conditions (the particle diffusion coefficient increases nearly as much as the kinematic viscosity). Therefore, the latter should also have the same transmission efficiency. Figure 9 shows the transformed transmission efficiencies for both flight situations, averaged over all experimental data, that is, coated and uncoated, sintered and not sintered. An exponential fitting function was added for the parameterization of the results.

Comparison of the two curves shows a slight shift toward a lower transmission efficiency for the high-Re case compared to low-Re case for a given particle diameter. As the high-Re case is the one with stronger turbulence inside the diffuser (Re up to 25 000), and the turbulent particle diffusion coefficient increases with increasing turbulence, the data suggest that turbulent diffusion is the dominant loss process in the inlet for small particles.

For the large DEHS particles, no inlet coating tests were necessary, because they are liquid and consequently bounce-off effects are not important. Figure 10 shows the measured transmission efficiencies for both flight situations.

When the CMAG was operated under slight overpressure (which was needed to inject the particles into the wind tunnel), particles larger than 6 μm could not

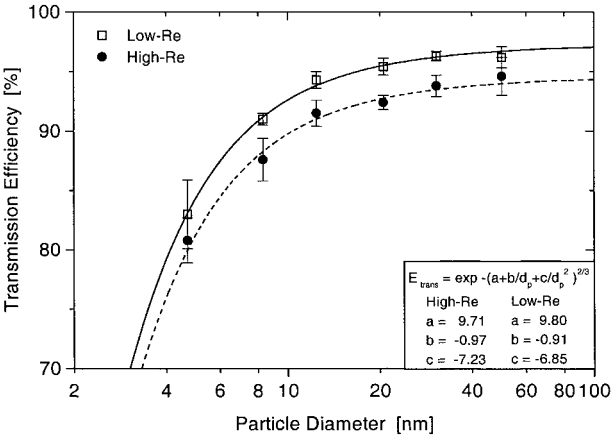

FIG. 9. Transformed, mean inlet transmission efficiencies for small particles. The solid and dashed lines represent exponential fitting functions to the experimental data. The chosen equation and respective coefficients are displayed in the lower-right corner. Here, E_{trans} gives the transmission efficiency as function of particle diameter d_p.

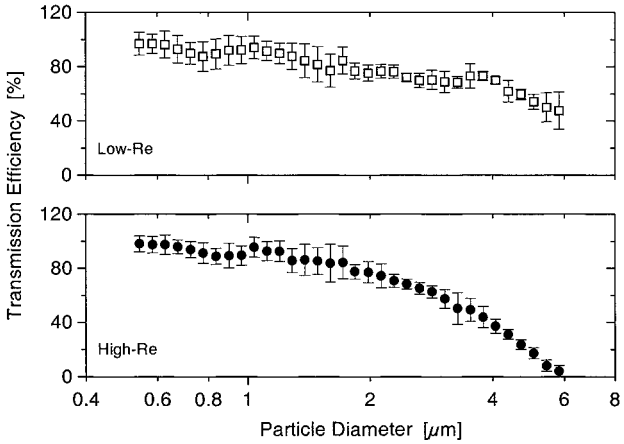

FIG. 10. Measured inlet transmission efficiencies for large particles.

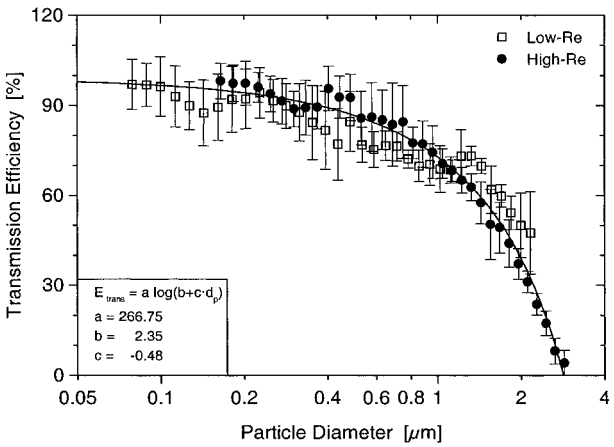

FIG. 11. Transformed, mean inlet transmission efficiencies for large particles. The solid line shows a logarithmic fitting function to both datasets (high Re and low Re). In the lower-right corner the respective equation and coefficients are displayed.

be generated in sufficiently high number concentrations. This is partly attributed to the large dilution ratios of up to 1:200 inside the mixing chamber. Therefore, no calibration data for particle sizes larger than 6 μm were obtained. In the range of 0.5–1.5 μm, transmission efficiencies lie just below 100% and decrease toward larger particle sizes. This decrease is partly related to turbulent deposition in the diffuser and partly to the backward-facing 6-mm tube in the inlet, which acts as separator. The large scattering of the data is again attributed to the particle generation and measurement method (cf. discussion of Fig. 6).

The results for the larger particles were transformed to real flight conditions in two steps. First, the aerodynamic diameter given by the APS was converted to Stokes diameters. Second, the averaged efficiency values at a certain particle diameter were transformed assuming identical particle Stokes numbers. For this transformation, a particle density of 1.55 g cm^{-3} for upper-tropospheric sulfuric acid aerosol was assumed (M_{H2SO4} = 60%; Steele and Hamill 1981). The obtained transmission efficiencies are shown in Fig. 11.

For the DEHS particles, a large shift toward smaller particle diameters due to the transformation can be seen. The reasons for this shift are the higher particle density and the much larger slip correction under real flight conditions. The measurement points have large standard deviations, but a definite decrease in transmission efficiency can be seen for the coarse particles. Although the raw data for the two cases show different transmission efficiencies at larger particle diameters, the data lie closely together after the transformation. A logarithmic fitting formula was applied to parameterize all data in one curve. It should be noted that comparing the two particle diameters of each flight situation, which have identical Stokes numbers, shows that also their transmission efficiencies are identical within the experimental errors. This suggests that the transmission efficiency for larger particles is mainly controlled by particle inertia and, consequently, the particle Stokes number is the appropriate particle property to describe the losses.

The large expansion angle of the CARIBIC inlet suggests flow separation in the diffuser. To check this, the inlet mock-up was disassembled after two or three calibration runs and the individual parts were visually inspected for particle deposition. Silver particles were found within the first 2 cm of the diffuser, by using a clean, white laboratory wiper. This is a hint with respect to flow separation and agrees well with modeling results given by Ram et al. (1995), who calculated regions of flow recirculations in diffusers.

For the large DEHS particles, the picture is more distinct. Over the first third of the inlet, DEHS was found round about on the diffuser wall already by visual inspection. Furthermore, there seemed to be a pattern of alternating higher and lower DEHS load. In the rear, parallel part of the inlet, no particle material could be found at the top and side walls of the inlet and only small amounts at the bottom. At the back of the 6-mm tube, which faces directly into the particle stream, no DEHS was found. This suggests that under flight conditions, particle losses caused by this tube will be minimal.

b. Transport efficiency

The transport efficiency accounts for particle losses in the sampling line between the inlet and the measurement devices. For CARIBIC, this tubing consists of a 2-m-long, 6-mm stainless steel tube with an inner diameter of 4 mm. The tube has four bends (2 at 90°, 2 at 45°). As the volume flow through this tube is between 7 and 11 L min^{-1}, dependent on the flight level conditions, Reynolds numbers are between 600 and 1700, indicating laminar flow. Furthermore, as only submicrometer particles are sampled, only laminar diffusive

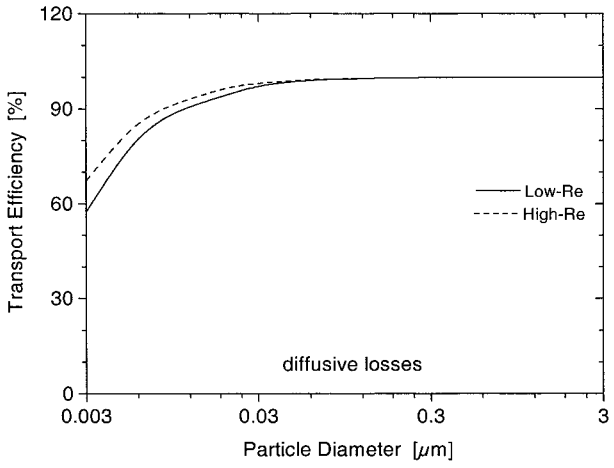

FIG. 12. Particle transport efficiency through the CARIBIC sampling line with respect to diffusive losses. Calculations were performed according to Eqs. (4) and (5), with a volume flow rate of 10 L min^{-1}, a mean temperature of 260 K, and pressures of 200 and 300 hPa, respectively.

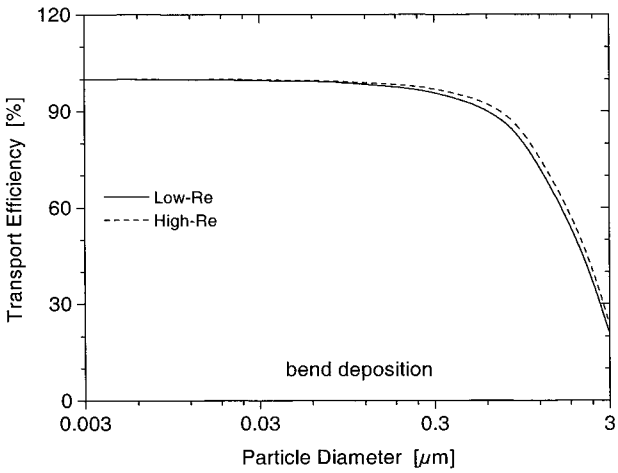

FIG. 13. Particle transport efficiency through the CARIBIC sampling line with respect to inertial deposition in tube bends. Calculations were performed according to Eq. (7), again, with a volume flow rate of 10 L min^{-1}, a mean temperature of 260 K, and pressures of 200 and 300 hPa, respectively.

and inertial deposition in bends must be considered for the transport losses in the CARIBIC sampling line.

The diffusive losses were calculated according to Eqs. (19)–(20), and (19)–(21) given in Willeke and Baron (1993) for the size range from 0.003 to 3 μm, which is given by the threshold diameters of the CPCs and the upper inlet cutoff. The equations represent an analytical function to measurement results of several authors and yield the transport efficiency, E_{diff}, by

$$E_{\text{diff}} = 0.819\exp(-3.657\mu) + 0.0975\exp(-22.305\mu) + 0.0325\exp(-56.961\mu) + 0.0154\exp(-107.62\mu) \quad \text{for } \mu > 0.02 \tag{4}$$

$$E_{\text{diff}} = 1 - 2.564\mu^{2/3} + 1.2\mu + 0.1767\mu^{4/3} \quad \text{for } \mu \le 0.02, \tag{5}$$

with μ defined as

$$\mu = \frac{\pi DL}{Q}. \tag{6}$$

Here, D is again the particle diffusion coefficient, L the length of the tube, and Q the volume flow through the tube. In Fig. 12, the transport efficiencies for both flight situations are shown. For particles larger than 50 nm, the transport efficiencies are nearly 100%. For the ultrafine particles they decrease rapidly and are below 70% for particles smaller than 4 nm. The difference in the two curves is mainly due to the different pressure conditions of the two flight situations.

For an estimation of the particles losses in the four tube bends of the CARIBIC sampling line, the formula given by Cheng and Wang (1981) has been used, which has been confirmed in 1987 by Pui et al. Since the formula was derived only for 90° bends and the CARIBIC sampling line has two 45° bends, the formula was expanded by a linear dependence of the transport efficiency on the bend angle α, as suggested by Crane and Evans (1977), to:

$$E_{\text{bend}} = \left(1 + \frac{\pi}{2R} + \frac{2}{3R^2}\right)\text{Stk}\frac{\alpha}{90}. \tag{7}$$

Here, E_{bend} is the particle transport efficiency, R the curvature ratio (bend radius divided by the tube radius), and Stk the particle Stokes number. The particle density has been assumed to 1.55 g cm^{-3} (sulfuric acid aerosol) again. The particle transport efficiencies obtained from Eq. (7) are shown in Fig. 13. Although the gas and particle velocities for the low-Re case are smaller than in the high-Re case, the former shows the greater particle losses. This is attributed to the larger slip correction caused by the lower pressure for the low-Re case.

c. Total sampling efficiency

Figure 14 summarizes all important particle loss processes in the CARIBIC inlet system. The total sampling efficiency results as the product of the inlet transmission, transport (i.e., diffusive losses and bend deposition), and aspiration efficiencies, whereby the latter was assumed to be 100% (cf. section 4). Losses of ultrafine particles are caused by turbulent diffusion in the inlet and diffusive processes during transport. The larger particle sampling efficiency is controlled by turbulent deposition in the diffuser and inertial separation at the 6-mm backward-facing tube in the inlet. It is important to note that the sampling efficiency for both flight situations are nearly equal. As these cases represent the two extremes of flight conditions, the inlet encounters during level flight, it can be assumed that the CARIBIC inlet has the

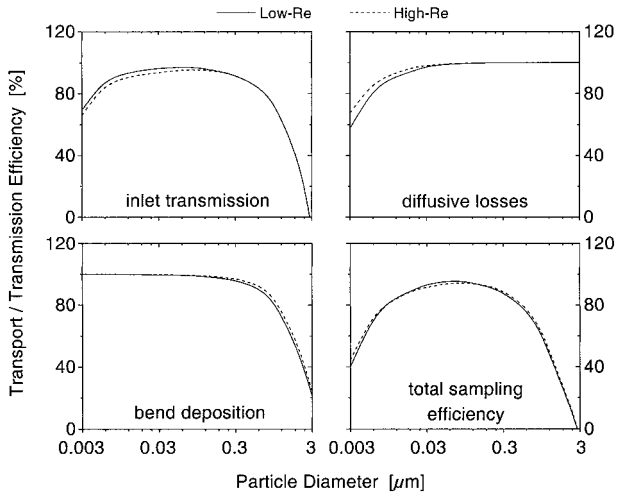

FIG. 14. Single inlet efficiencies and resulting total sampling efficiency of the CARIBIC inlet system. The diffusive losses and deposition in bends were calculated, whereas the inlet transmission shows experimental results.

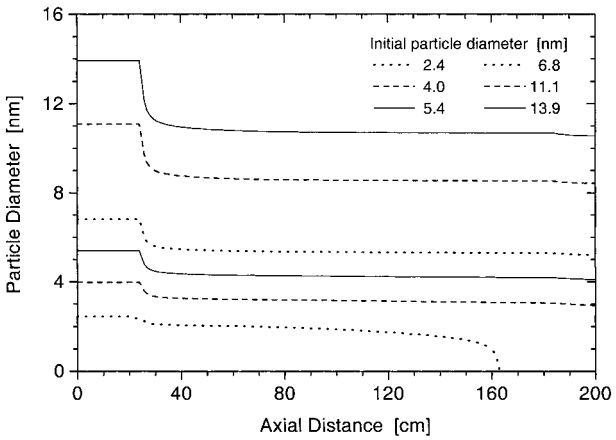

FIG. 15. Change in particle ''wet'' diameter as a function of axial distance along the mean sampling streamline. Curves were calculated with the MADMAcS model for sulfuric acid/water particles and an initial ambient relative humidity of 30%.

same sampling efficiency at all cruising altitudes of the B-767.

d. Particle modification

Besides the aforementioned loss processes affecting particle number concentration, modifications of the particle size distribution due to aerosol dynamical processes in the inlet/sampling system must be accounted for. The most prominent process in this context is the evaporation of particle material. It is caused by the strong heating from upper-tropospheric temperatures around 223 K to room temperature inside the measurement container and leads to a decrease of particle diameter. As ultrafine particle concentrations in CARIBIC are derived by subtracting the number concentrations of two CPCs with different lower threshold diameters (4 and 12 nm), it is particularly important to know to which extent evaporation can cause small particles (4–5 nm) to shrink below this size range, or particles larger than 12 nm to enter it.

The evaporation of particle material in the CARIBIC sampling line was studied using the aerosol dynamics model MADMAcS (Wilck and Stratmann 1997; Wilck 1999). Since the de-icing and dynamic heating is considered to be much smaller than the heating in the sampling line (cf. section 4), only the second effect was modeled. First, the temperature field in the sampling line was simulated using the general fluid dynamics and transport code COMPACT-2D (Innovative Research 1996). The heating occurs in two steps: 25 cm downstream from the tube inlet, where the sampling line enters the cargo compartment, the air is heated to about 288 K; and 160 cm farther downstream to 298 K in the aerosol rack unit. In the simulation a pressure of 200 hPa and a flow rate of 10 L min^{-1} were assumed. The evaporation process was then studied along streamlines through this temperature field using an implicit ordinary differential equations solver (Hindmarsh 1983), which is well suited for solving the stiff set of equations resulting from rapid evaporation processes. The lognormal MADMAcS model was used in a ''pseudo-monodisperse'' condition by setting the initial geometric standard deviation of an assumed lognormal distribution to 1.01. The particles were assumed to be sulfuric acid/water particles; their water content was assumed to be in equilibrium with the ambient relative humidity outside the aircraft. The thermodynamics of the water/sulfuric acid mixture was described by the parameterization of Zeleznik (1991).

Like most current aerosol models, usually MADMAcS does not explicitly treat water condensation/evaporation processes of submicrometer particles at undersaturated conditions. These processes are rather covered by the assumption of permanent water–gas-particle equilibrium. To test the validity of this assumption for the fast evaporation processes in the sampling line, comparisons between an explicit binary evaporation model and the equilibrium model have been carried out with MADMAcS. The maximum deviation found was a time lag of approximately 1 ms caused by the explicit treatment of water evaporation. The final size and composition of the particles at the outlet of the sampling line were identical in both models. Therefore, the equilibrium assumption was found to be justified.

Figure 15 shows the change of the particle ''wet'' diameter, that is, the diameter the particles have ambient RH in contrast to the ''dry'' diameter they would have at RH = 0, as a function of axial distance along the mean sample streamline of the CPCs. The rapid decrease of particle diameter due to water evaporation at the first heating step ($z \sim 30$ cm) is clearly seen. The relative humidity in the flow after this heating step is already so low that further heating to 298 K (at $z \sim 185$ cm)

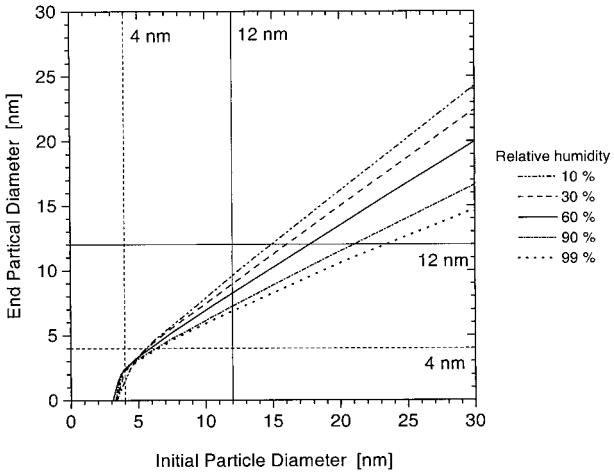

FIG. 16. Comparison of particle ''wet'' diameter upstream (''initial'') and downstream (''end'') the sampling line. The curves represent different ambient relative humidities outside the aircraft. Vertical and horizontal straight lines denote the lower detection limits of the two CPCs used in phase 1 of CARIBIC.

causes only little additional water evaporation. Sulfuric acid evaporation is a much slower process. It occurs steadily after the first heating step and accelerates after the second, but hardly affects the particle diameter except for the smallest particles which may even evaporate completely. Note that the ambient sulfuric acid gas phase concentration had been set to zero in order to obtain an upper estimate for sulfuric acid losses from particles.

In Fig. 16, the change in particle wet diameter upstream and downstream the sampling line is summarized for different initial diameters and ambient relative humidities. The figure further shows horizontal and vertical lines indicating the ''measuring window'' defined by the CPC threshold diameters of 4 and 12 nm. It can be seen that particles measured at the lower threshold diameter of 4 nm correspond to original particle diameters of 5–7 nm. Particles registered at the upper threshold diameter (12 nm) may originally have been as large as 20 nm. However, most of this effect is due to water evaporation. Evaporation of the more ''persistent'' particle component, sulfuric acid, plays a negligible role except for the smallest particles well below the lower threshold diameter of 4 nm in the CARIBIC setup. Consequently, particles observed in the ultrafine particle size range are not necessarily freshly nucleated. It is likewise possible that these particles shrunk into the ultrafine particle size window defined by the CPCs.

6. Conclusions

In this study, we described a new aircraft-borne diffuser type aerosol inlet system, which is flown regularly in the CARIBIC project. The sampling properties of this diffuser-type inlet have been studied in a wind-tunnel experiment utilizing a similarity approach. This approach is based on the assumption that flow and particle transport are similar if dimensionless properties such as the Reynolds number (flow field), particle Schmidt number (diffusive particle transport), and particle Stokes number (inertial effects) are identical during flight and in the laboratory. As result, we presented, for the first time, a size-resolved inlet transmission efficiency in the particle diameter range from 0.003 to 3 μm. The aspiration efficiency of our inlet is assumed to be 100%. Furthermore, the particle transport efficiencies of the sampling line between the inlet and the measurement container have been calculated with respect to diffusion and inertial deposit in bends.

The obtained total sampling efficiency is 83%, 95%, and 81% for 10, 100, and 500-nm particles, respectively. For ultrafine particles (for CARIBIC: $D_p < 12$ nm), sampling efficiency rapidly decreases (55% at 4 nm) due to turbulent diffusion in the inlet diffuser and diffusive losses in the sampling line. The upper cutoff diameter of the inlet system is determined by turbulent deposition in the diffuser and the backward-facing sampling tube in the inlet which acts as a separator.

The modification of the particle size distribution due to evaporation caused by rapid heating in the sampling line has been studied with the MADMAcS aerosol dynamics model. The investigations were carried out for sulfuric acid/water particles at different ambient relative humidities. It was found that a significant amount of water is evaporated from the sampled particles (considerable decrease of the ''wet'' diameter), whereas sulfuric acid evaporation is so slow that particles larger than 4 nm lose only a negligible amount of their sulfuric acid mass during transport. Consequently, particles are entering the CPCs at their ''dry'' diameters (the diameter they would have at RH = 0), that is, particles observed in the smallest measured particle size range might not be freshly nucleated. It is likewise possible that these particles shrunk into the ultrafine particle size window.

The obtained results reduce the uncertainties in particle number concentrations measured using the CARIBIC inlet and are therefore an essential part of the data interpretation inside the CARIBIC project.

Acknowledgments. We thank the LTU International Airways for financial and logistic support. This work is financially supported by the Environmental Technologies RTD Program of the Commission of the European Communities DG XII under Contract ENV4-CT95-0006.

REFERENCES

Baumgardner, D., and B. Huebert, 1993: The airborne aerosol inlet workshop: Meeting report. *J. Aerosol Sci.*, **24,** 835–846.

——, ——, and C. Wilson 1991: Meeting review: Airborne aerosol inlet workshop. NCAR Tech. Note TN-362 + 1A, 288 pp.

Brenninkmeijer, C. A. M., and Coauthors, 1999: CARIBIC—Civil aircraft for global measurement of trace gases and aerosols in

the tropopause region. *J. Atmos. Oceanic Technol.,* **16,** 1373–1383.

Cain, S. A., and M. Ram, 1998: Numerical simulation studies of the turbulent airflow through a shrouded airborne aerosol sampling probe and estimation of the minimum sampler transmission efficiency. *J. Aerosol Sci.,* **29,** 1145–1156.

——, ——, and S. Woodward, 1998: Qualitative and quantitative wind-tunnel measurements of the airflow through a shrouded airborne aerosol sampling probe. *J. Aerosol Sci.,* **29**, 1157–1169.

Cheng, Y.-S., and H.-S. Yeh, 1979: Particle bounce in cascade impactors. *Environ. Sci. Technol.,* **13**, 1392–1396.

——, and C. S. Wang, 1981: Motion of particles in bends of circular pipes. *Atmos. Environ.,* **15,** 301–306.

Crane, R. I., and R. L. Evans, 1977: Inertial deposition of particles in a bend pipe. *J. Aerosol Sci.,* **8,** 161–170.

Driscoll, W. G., and W. Vaughan, Eds., 1978: *Handbook of Optics.* McGraw-Hill, 1600 pp.

Geller, A. S., D. J. Rader, and S. N. Kempka, 1993: Calculation of particle concentration around aircraft-like geometries. *J. Aerosol Sci.,* **24,** 823–834.

Hindmarsh, A. C., 1983: Odepack, a systemized collection of ODE solvers. *IMACS Transaction on Scientific Computing,* R. S. Stepleman, Ed., 55–64.

Holton, J. R., P. H. Haynes, M. E. McIntyre, A. R. Douglass, R. B. Rood, and L. Pfister, 1995: Stratosphere–troposphere exchange. *Rev. Geophys.,* **33,** 403–439.

Hudson, J. G., and P. R. Frisbie, 1991: Cloud condensation nuclei near marine stratus. *J. Geophys. Res.,* **96,** 20 795–20 908.

Huebbert, B. J., G. Lee, and W. L. Warren, 1990: Airborne aerosol inlet passing efficiency measurements. *J. Geophys. Res.,* **95,** 16 369–16 381.

Innovative Research, 1996: *Reference Manual for COMPACT-2D Version 4.0.* Innovative Research, Inc.

Ivie, J. J., L. J. Forney, and R. L. Roach, 1990: Supersonic particle probes: Measurement of internal wall losses. *Aerosol Sci. Technol.,* **13,** 368–385.

King, W. D., 1984: Air flow and particle trajectories around aircraft fuselages. I: Theory. *J. Atmos. Oceanic Technol.,* **1,** 5–13.

——, 1985: Air flow and particle trajectories around aircraft fuselages. Part III: Extensions to particles of arbitrary shape. *J. Atmos. Oceanic Technol.,* **2,** 539–547.

——, 1986: Air flow and particle trajectories around aircraft fuselages. IV: Orientation of ice crystals. *J. Atmos. Oceanic Technol.,* **3,** 433–440.

——, D. E. Turvey, D. Williams, and D. J. Llewellyn, 1984: Air flow and particle trajectories around aircraft fuselages. II: Measurements. *J. Atmos. Oceanic Technol.,* **1,** 14–21.

Laucks, M. L., and C. H. Twohy, 1998: Size-dependent collection efficiency of an airborne counterflow virtual impactor. *Aerosol Sci. Technol.,* **28,** 40–61.

Lin, H., and J. Heintzenberg, 1995: A theoretical study of the counterflow virtual impactor. *J. Aerosol Sci.,* **26,** 903–914.

Mahlman, J. D., 1997: Dynamics of transport processes in the upper troposphere. *Science,* **276,** 1079–1083.

Marenco, A., and Coauthors, 1998: Measurement of ozone and water vapor by Airbus in-service aircraft: The MOZAIC airborne program: An overview. *J. Geophys. Res.,* **103,** 25 631–25 642.

McFarland, A. R., C. A. Ortiz, M. E. Moore, R. E. DeOette Jr., and S. Somsundaram, 1989: A shrouded aerosol sampling probe. *Environ. Sci. Technol.,* **23,** 1487–1492.

Murphy, D. M., and M. E. Schein, 1998: Wind-tunnel tests of a shrouded aircraft inlet. *Aerosol Sci. Technol.,* **28,** 33–39.

Porter, J. N., A. D. Clarke, G. Ferry, and R. F. Pueschel, 1992: Aircraft studies of size-dependent aerosol sampling through inlets. *J. Geophys. Res.,* **97,** 3815–3824.

Pui, D. Y. H., F. Romay-Novas, and B. Y. H. Liu, 1987: Experimental study of particle deposition in bends of circular cross-section. *Aerosol Sci. Technol.,* **7,** 301–315.

Radke, L. F., and J. E. Dye, 1991: Aircraft electrical charge: An aerosol inlet issue. NCAR Tech. Note TN-362 + 1A, 288 pp.

Ram, M., S. A. Cain, and D. B. Taulbee, 1995: Design of a shrouded probe for airborne aerosol sampling in a high velocity airstream. *J. Aerosol Sci.,* **26,** 945–962.

Romay, F. J., D. Y. H. Pui, T. J. Smith, N. D. Ngo, and J. H. Vincent, 1996: Corona discharge effects on aerosol sampling efficiency. *Atmos. Environ.,* **30,** 2607–2613.

Scheibel, H. G., and J. Porstendörfer, 1983: Generation of monodisperse Ag and NaCl aerosols with particle diameters between 2 and 300 nm. *J. Aerosol Sci.,* **14,** 113–126.

Schmidt-Ott, A., 1988: New approaches to in situ characterization of ultrafine agglomerates. *J. Aerosol Sci.,* **19,** 553–563.

Schröder, F., and J. Ström, 1997: Aircraft measurements of sub micrometer aerosol particles (>7 nm) in the midlatitude free troposphere and tropopause region. *Atmos. Res.,* **44,** 333–356.

Sheridan, P. J., and R. B. Norton, 1998: Determination of the passing efficiency for aerosol chemical species through a typical aircraft-mounted, diffuser-type aerosol inlet system. *J. Geophys. Res.,* **103,** 8215–8225.

Soderman, P. T., N. L. Hazen, and W. H. Brune, 1991: On the aerodynamic design of gas and aerosol samplers for aircraft. NCAR Tech. Note TN-362 + 1A, 288 pp.

Steele, H. M., and P. Hamill, 1981: Effects of temperature and humidity on the growth and optical properties of sulphuric acid-water droplets in the stratosphere. *J. Aerosol Sci.,* **12,** 517–528.

Torgeson, W. L., and S. C. Stern, 1966: An aircraft impactor for determining the size distributions of tropospheric aerosol. *J. Appl. Meteor.,* **5,** 205–210.

Twohy, C. H., 1998: Model calculations and wind-tunnel testing of an isokinetic shroud for high-speed sampling. *Aerosol Sci. Technol.,* **29,** 261–280.

——, and D. Rogers, 1993: Airflow and water-drop trajectories at instrument sampling points around the Beechcraft King Air and Lockheed Electra. *J. Atmos. Oceanic Technol.,* **10,** 566–578.

Weber, R. J., A. D. Clark, M. Litchy, J. Li, G. Kok, R. D. Schillawski, and P. H. McMurry, 1998: Spurious aerosol measurements when sampling from aircraft in the vicinity of clouds. *J. Geophys. Res.,* **103,** 28 337–28 346.

Wilck, M., 1999: Modal modelling of multicomponent aerosols. Ph.D. thesis, Universität Leipzig, 137 pp. [Available from Martin Wilck, Institute for Tropospheric Research, Permoser Str. 15, D-04318, Leipzig, Germany; also available from martin@tropos.de.]

——, and F. Stratmann, 1997: A 2-D multicomponent aerosol model and its application to laminar flow reactors. *J. Aerosol Sci.,* **28,** 959–972.

Willeke, K., and P. A. Baron, 1993: *Aerosol Measurements: Principles, Techniques and Applications.* Van Nostrand Reinhold, 876 pp.

Zeleznik, F. J., 1991: Thermodynamic properties of the aqueous sulfuric acid system to 350K. *J. Phys. Chem. Ref. Data,* **20,** 1157–1200.